Electronic supplementary information (ESI)

to

Collision-induced gas-phase reactions of perhalogenated *closo*-dodecaborate clusters
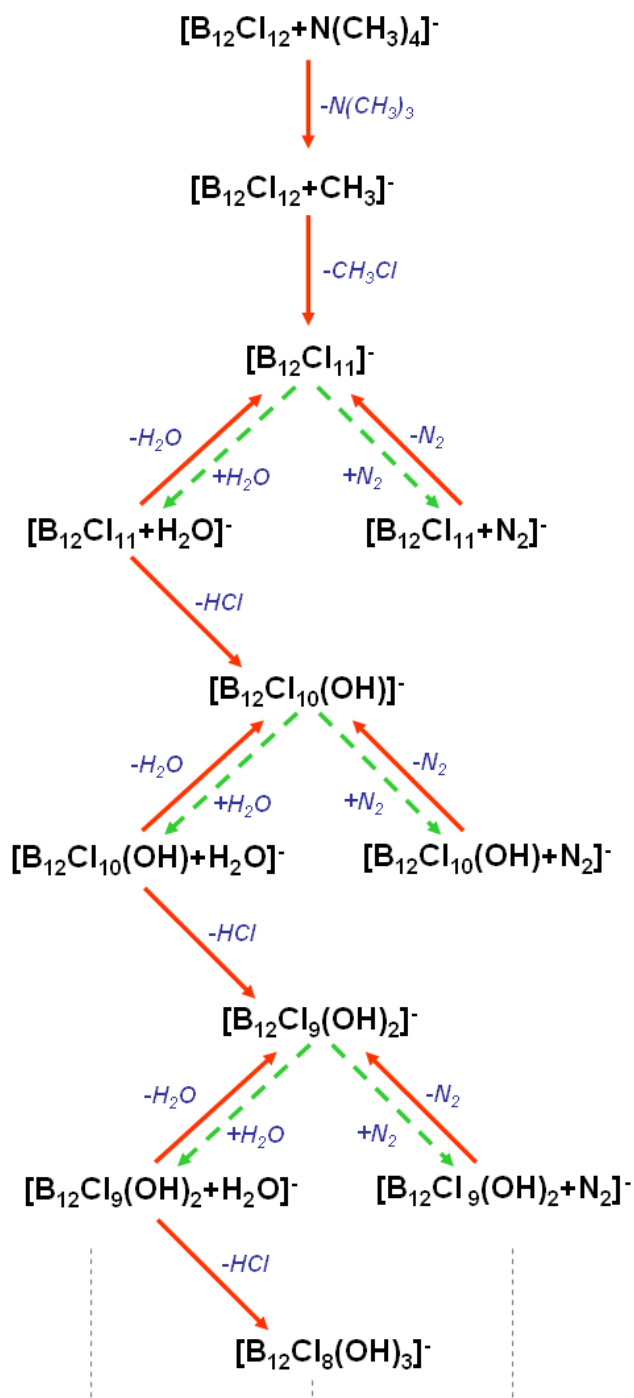
- A comparative study -

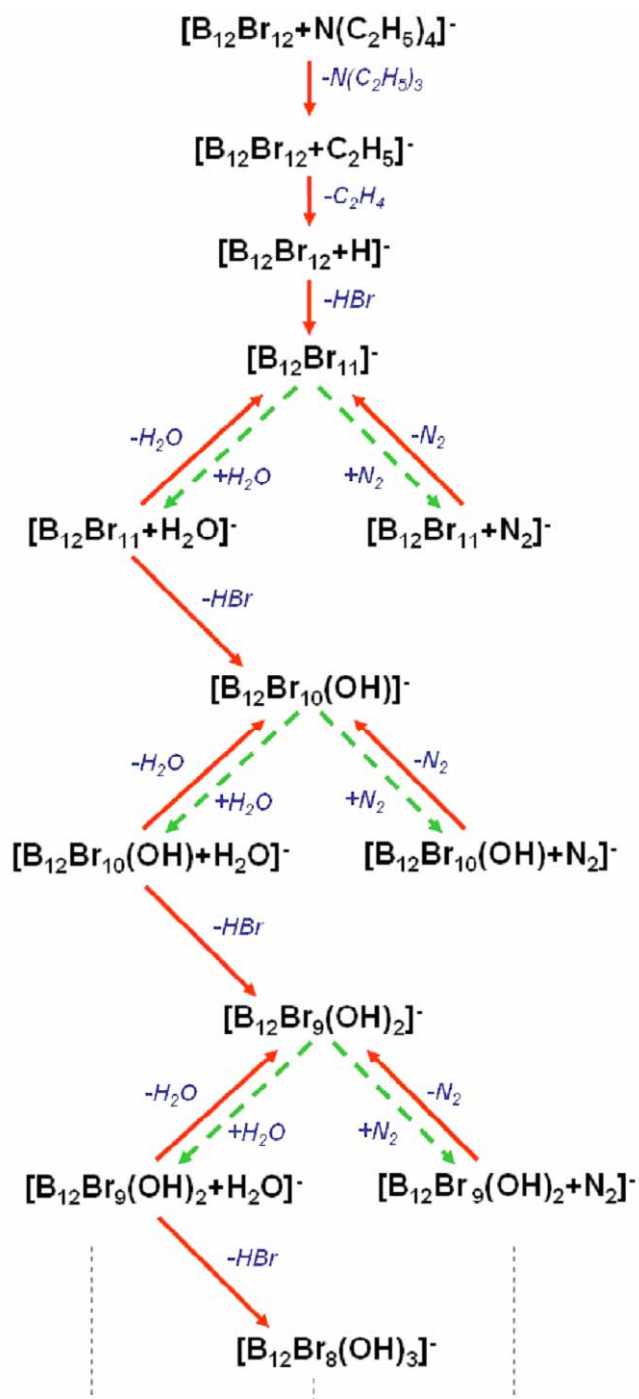**Jonas Warneke,[a] Thomas Dülcks,*[a] Carsten Knapp,*[b], Detlef Gabel[a]**

[a]   Fachbereich 2 Chemie
        Universität Bremen
        Leobener Strasse, NW2
        D-28359 Bremen, Germany.
        E-mail: duelcks@uni-bremen.de
        Tel: +49-421-218-62820
        Fax: +49-421-218-63102

[b]   Institut für Anorganische und Analytische Chemie
        Albert-Ludwigs Universität Freiburg
        Albertstr. 21
        79104 Freiburg i. Br., Germany.
        E-mail: carsten.knapp@ac.uni-freiburg.de
        Tel: +49-761-203-6150
        Fax: +49-761-203-6001

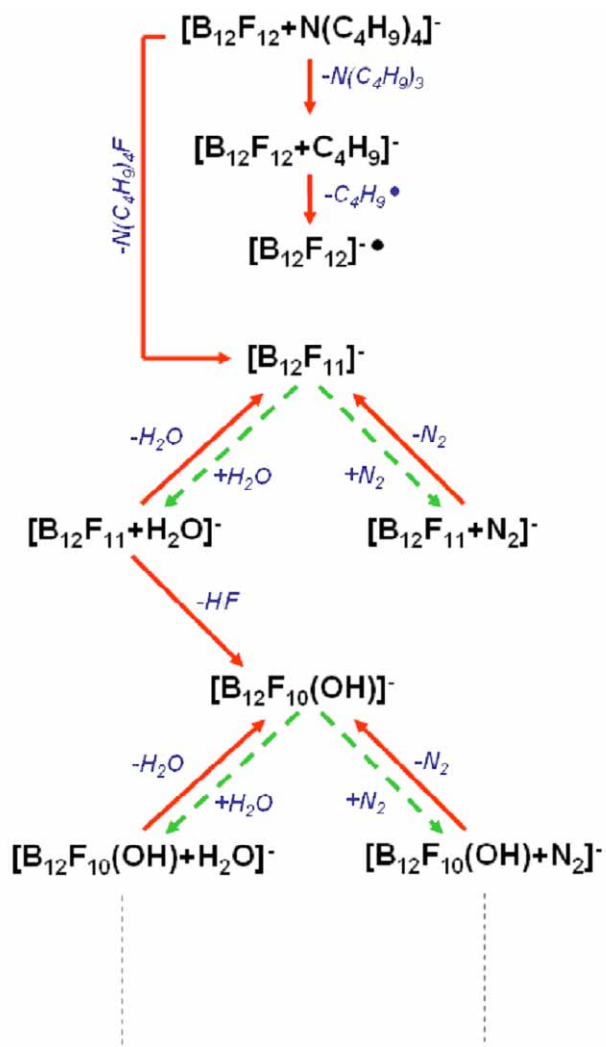**S1. Additional mass spectra and other information for chapter 3.1**

$[B_{12}Cl_{12}+N(CH_3)_4]^-$

$-N(CH_3)_3$

$[B_{12}Cl_{12}+CH_3]^-$

$-CH_3Cl$

$[B_{12}Cl_{11}]^-$

$-H_2O$　$+H_2O$　$+N_2$　$-N_2$

$[B_{12}Cl_{11}+H_2O]^-$　　$[B_{12}Cl_{11}+N_2]^-$

$-HCl$

$[B_{12}Cl_{10}(OH)]^-$

$-H_2O$　$+H_2O$　$+N_2$　$-N_2$

$[B_{12}Cl_{10}(OH)+H_2O]^-$　　$[B_{12}Cl_{10}(OH)+N_2]^-$

$-HCl$

$[B_{12}Cl_9(OH)_2]^-$

$-H_2O$　$+H_2O$　$+N_2$　$-N_2$

$[B_{12}Cl_9(OH)_2+H_2O]^-$　　$[B_{12}Cl_9(OH)_2+N_2]^-$

$-HCl$

$[B_{12}Cl_8(OH)_3]^-$

Scheme S1. Detailed reaction diagram for the fragmentation of $[B_{12}Cl_{12} + N(CH_3)_4]^-$ in an ion trap applying excitation energy (Red arrow: Reaction induced by excitation; green arrow: Spontaneous reaction without applying excitation energy).

$[B_{12}Br_{12}+N(C_2H_5)_4]^-$

$\downarrow -N(C_2H_5)_3$

$[B_{12}Br_{12}+C_2H_5]^-$

$\downarrow -C_2H_4$

$[B_{12}Br_{12}+H]^-$

$\downarrow -HBr$

$[B_{12}Br_{11}]^-$

$-H_2O$ $+H_2O$ $+N_2$ $-N_2$

$[B_{12}Br_{11}+H_2O]^-$ $[B_{12}Br_{11}+N_2]^-$

$-HBr$

$[B_{12}Br_{10}(OH)]^-$

$-H_2O$ $+H_2O$ $+N_2$ $-N_2$

$[B_{12}Br_{10}(OH)+H_2O]^-$ $[B_{12}Br_{10}(OH)+N_2]^-$

$-HBr$

$[B_{12}Br_9(OH)_2]^-$

$-H_2O$ $+H_2O$ $+N_2$ $-N_2$

$[B_{12}Br_9(OH)_2+H_2O]^-$ $[B_{12}Br_9(OH)_2+N_2]^-$

$-HBr$

$[B_{12}Br_8(OH)_3]^-$

Scheme S2. Detailed reaction diagram for the fragmentation of $[B_{12}Br_{12} + N(C_2H_5)_4]^-$ in an ion trap applying excitation energy (Red arrow: Reaction induced by excitation; green arrow: Spontaneous reaction without applying excitation energy).

$[B_{12}I_{12}+N(C_3H_7)_4]^-$

$\downarrow -N(C_3H_7)_3$

$[B_{12}I_{12}+C_3H_7]^-$

$\downarrow -C_3H_6$

$[B_{12}I_{12}+H]^-$

$\downarrow -HI$

$[B_{12}I_{11}]^-$

$-H_2O$ $+H_2O$ $+N_2$ $-N_2$

$[B_{12}I_{11}+H_2O]^-$ $[B_{12}I_{11}+N_2]^-$

$-HI$

$[B_{12}I_{10}(OH)]^-$

$-H_2O$ $+H_2O$ $+N_2$ $-N_2$

$[B_{12}I_{10}(OH)+H_2O]^-$ $[B_{12}I_{10}(OH)+N_2]^-$

$-HI$

$[B_{12}I_9(OH)_2]^-$

$-H_2O$ $+H_2O$ $+N_2$ $-N_2$

$[B_{12}I_9(OH)_2+H_2O]^-$ $[B_{12}I_9(OH)_2+N_2]^-$

$-HI$

$[B_{12}I_8(OH)_3]^-$
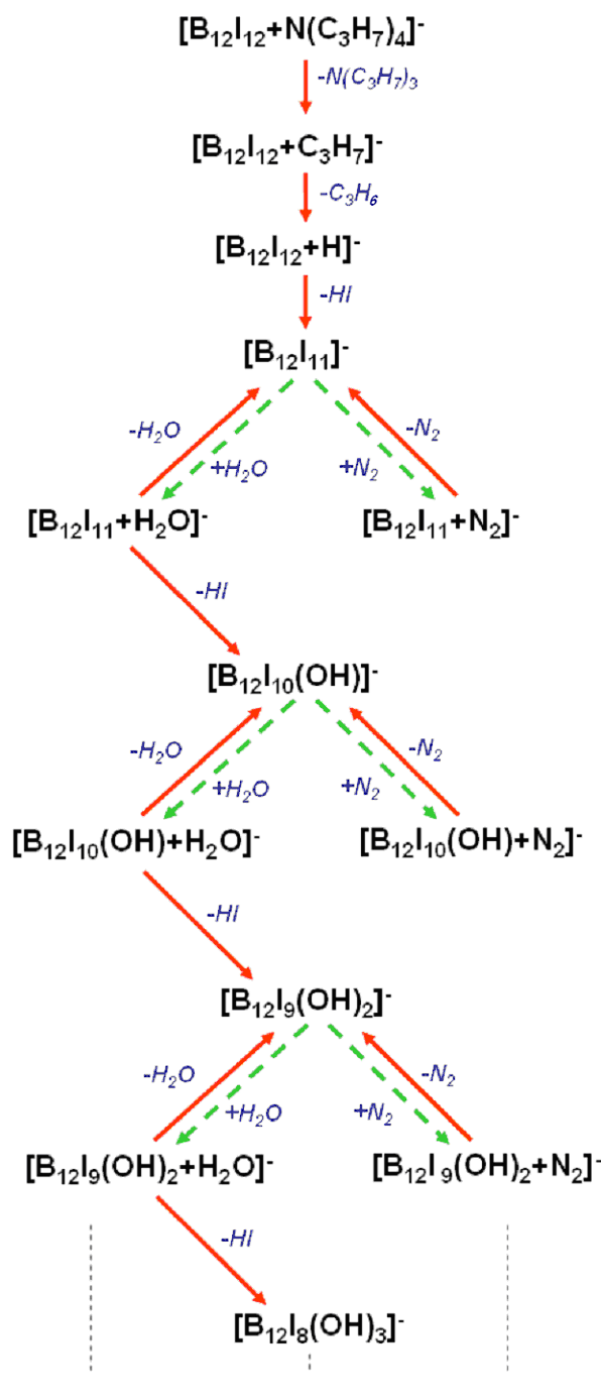
Scheme S3. Detailed reaction diagram for the fragmentation of $[B_{12}I_{12} + N(C_3H_7)_4]^-$ in an ion trap applying excitation energy (Red arrow: Reaction induced by excitation; green arrow: Spontaneous reaction without applying excitation energy).

$[B_{12}F_{12}+N(C_4H_9)_4]^-$

$-N(C_4H_9)_3$

$[B_{12}F_{12}+C_4H_9]^-$

$-C_4H_9^\bullet$

$[B_{12}F_{12}]^{-\bullet}$

$-N(C_4H_9)_4F$

$[B_{12}F_{11}]^-$

$-H_2O$ $+H_2O$ $+N_2$ $-N_2$

$[B_{12}F_{11}+H_2O]^-$ $[B_{12}F_{11}+N_2]^-$

$-HF$

$[B_{12}F_{10}(OH)]^-$

$-H_2O$ $+H_2O$ $+N_2$ $-N_2$

$[B_{12}F_{10}(OH)+H_2O]^-$ $[B_{12}F_{10}(OH)+N_2]^-$

Scheme S4. Detailed reaction diagram for the fragmentation of $[B_{12}F_{12}+N(C_4H_9)_4]^-$ in an ion trap applying excitation energy (Red arrow: Reaction induced by excitation; green arrow: Spontaneous reaction without applying excitation energy).
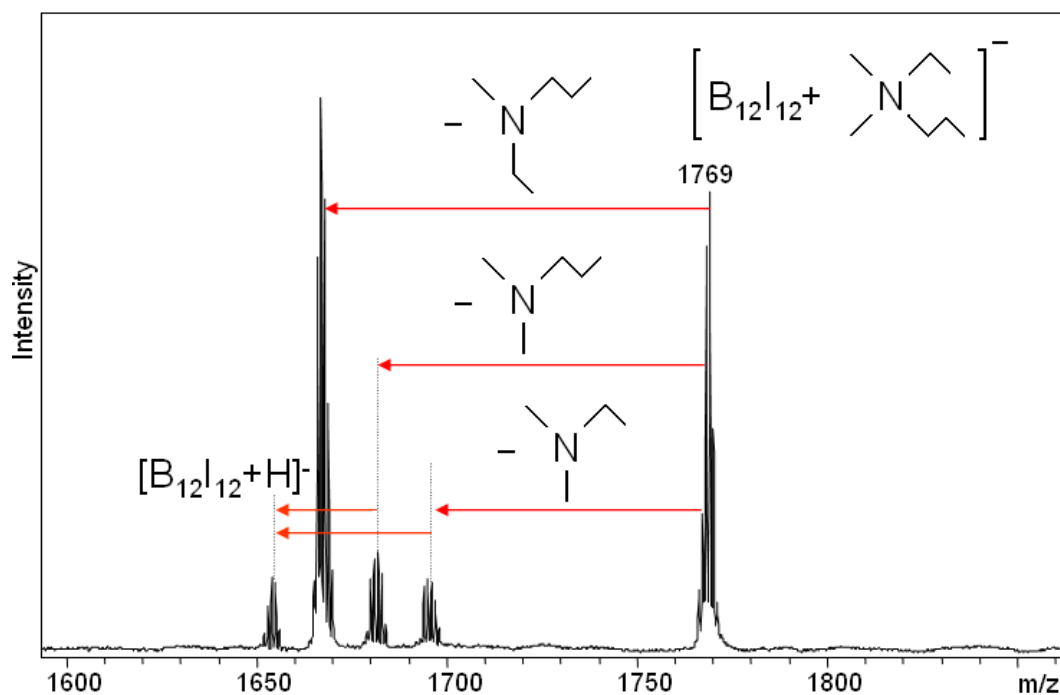
Fig. S1. ESI mass spectrum showing the fragments of the ion $[B_{12}I_{12} + N(CH_3)_2(C_2H_5)(C_3H_7)]^-$ in a tandem-MS experiment.
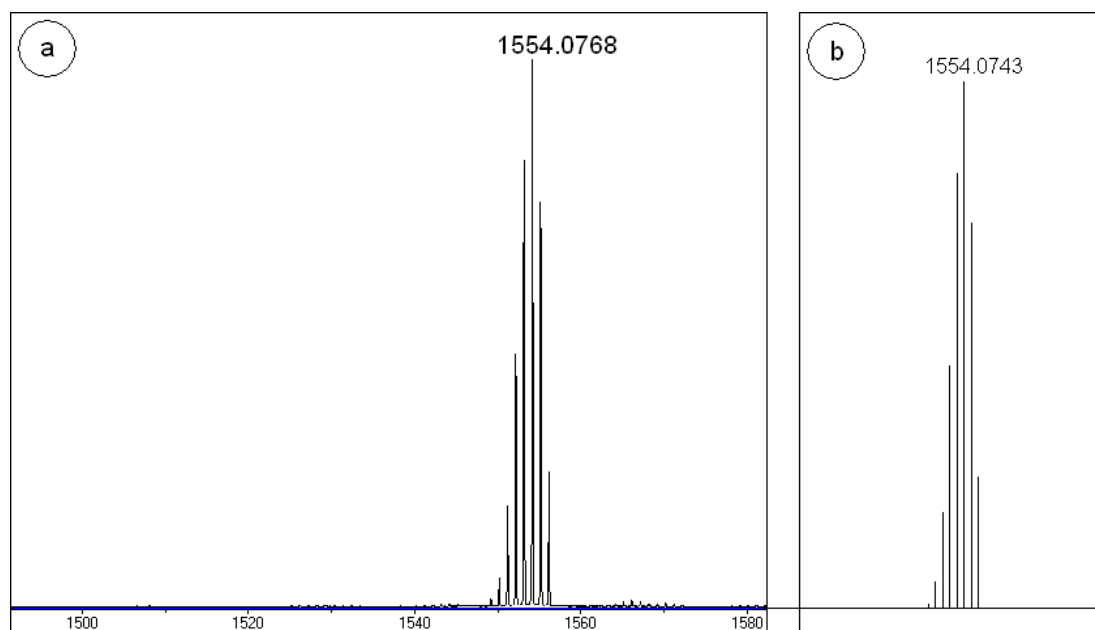
Fig. S2. a) ESI-ToF accurate mass measurement, shown m/z-range 1480−1580. The difference of the detected $[^{11}B_{12}{}^{127}I_{11}{}^{14}N_2]^-$ -signal to the theoretical value is −1.4 ppm. b) Simulated isotopic pattern of $[B_{12}I_{11}N_2]^-$.
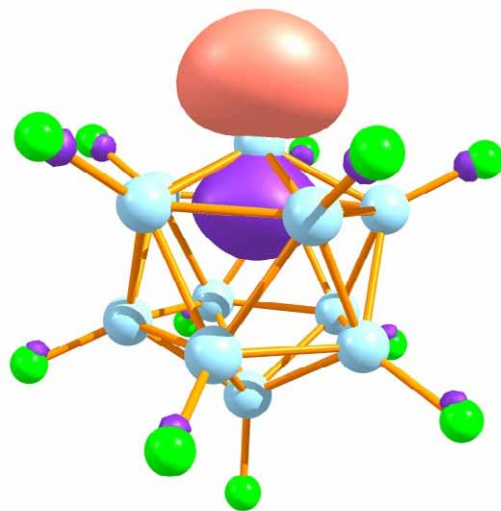
Fig. S3. Calculated structure and LUMO of $[B_{12}F_{11}]^-$ at the PBE0/def2-TZVPP level.

Increasing ion trap dwell time
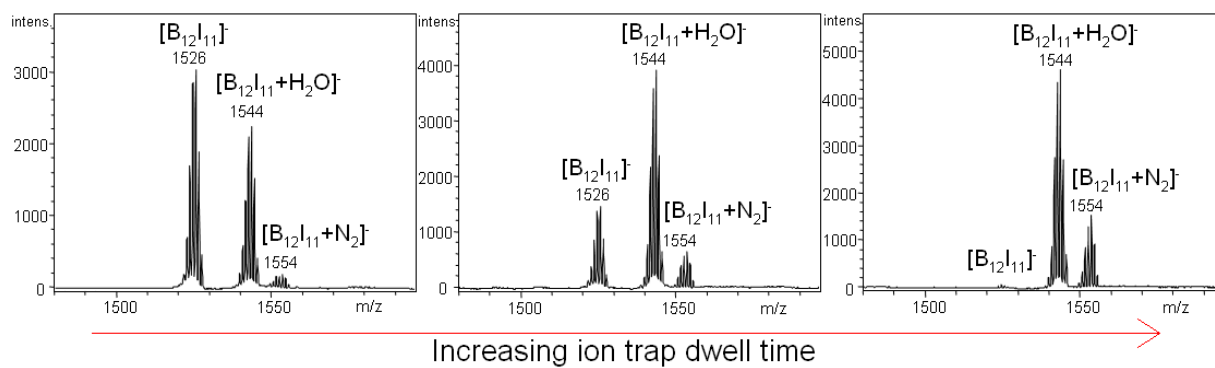
Fig. S4. ESI mass spectra showing the progress of the adduct formation of $[B_{12}I_{11}]^-$ with water and nitrogen over time.
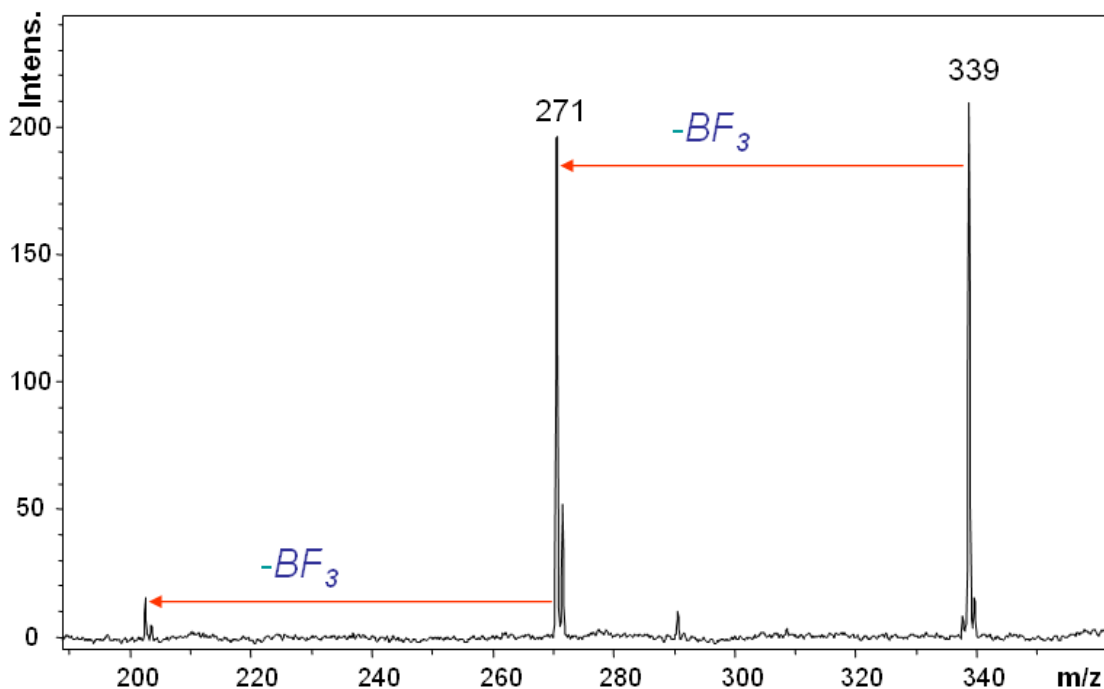
Fig. S5. ESI-mass-spectrum showing the excitation of $[B_{12}F_{11}]^-$ (m/z = 339) in the ion trap.

**Tab.S1: Total energies including ZPE (hartree) for $[B_{12}X_{11}]^-$ and $[B_{12}X_{11}N_2]^-$**

Ion	Total Energy [hartree]	N_2 Binding energy [kJ mol^{-1}]	d(B-N) [pm]	d(N-N) [pm]
$[B_{12}F_{11}]^-$	-1396.371045			
$[B_{12}F_{11}N_2]^-$	-1505.875270	-166.9	144.6	110.1
$[B_{12}Cl_{11}]-$	-5359.310777			
$[B_{12}Cl_{11}N_2]^-$	-5468.808685	-150.3	147.0	109.4
$[B_{12}Br_{11}]^-$	-28611.036872			
$[B_{12}Br_{11}N_2]^-$	-28720.532230	-143.6	147.9	109.3
$[B_{12}I_{11}]^-$	-3573.466767			
$[B_{12}I_{11}N_2]^-$	-3682.956221	-128.1	148.9	109.2
N_2	-109.440675			109.0

All calculated structures (PBE0/def2-TZVPP) have C_{5v} symmetry and are true minima on the respective hypersurfaces as shown by the absence of imaginary frequencies. Exemplarily, the calculated structures of $[B_{12}F_{11}]^-$ and $[B_{12}F_{11}N_2]^-$ are shown in Fig. S6.
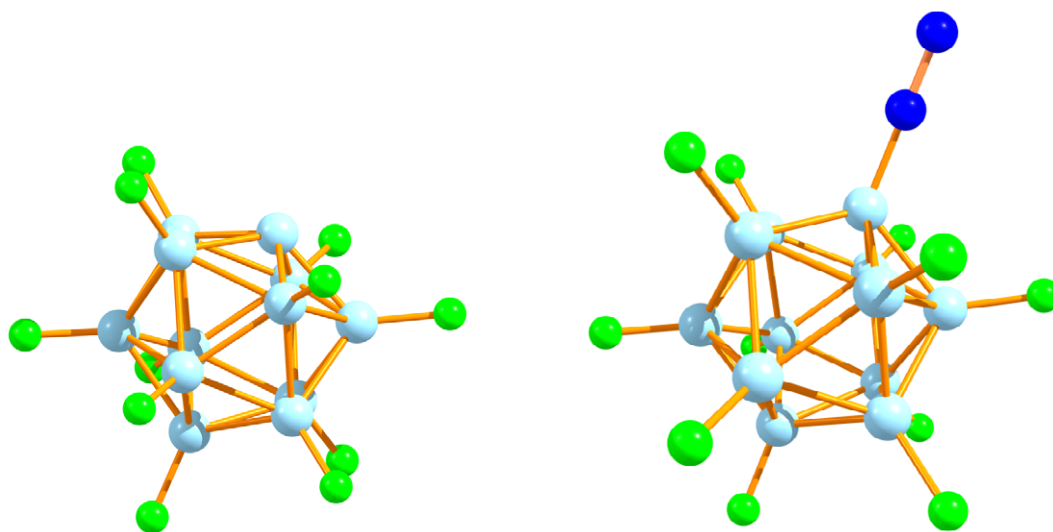
**Fig. S6.** Calculated structures (PBE0/def2-TZVPP level) of $[B_{12}F_{11}]^-$ and $[B_{12}F_{11}N_2]^-$.
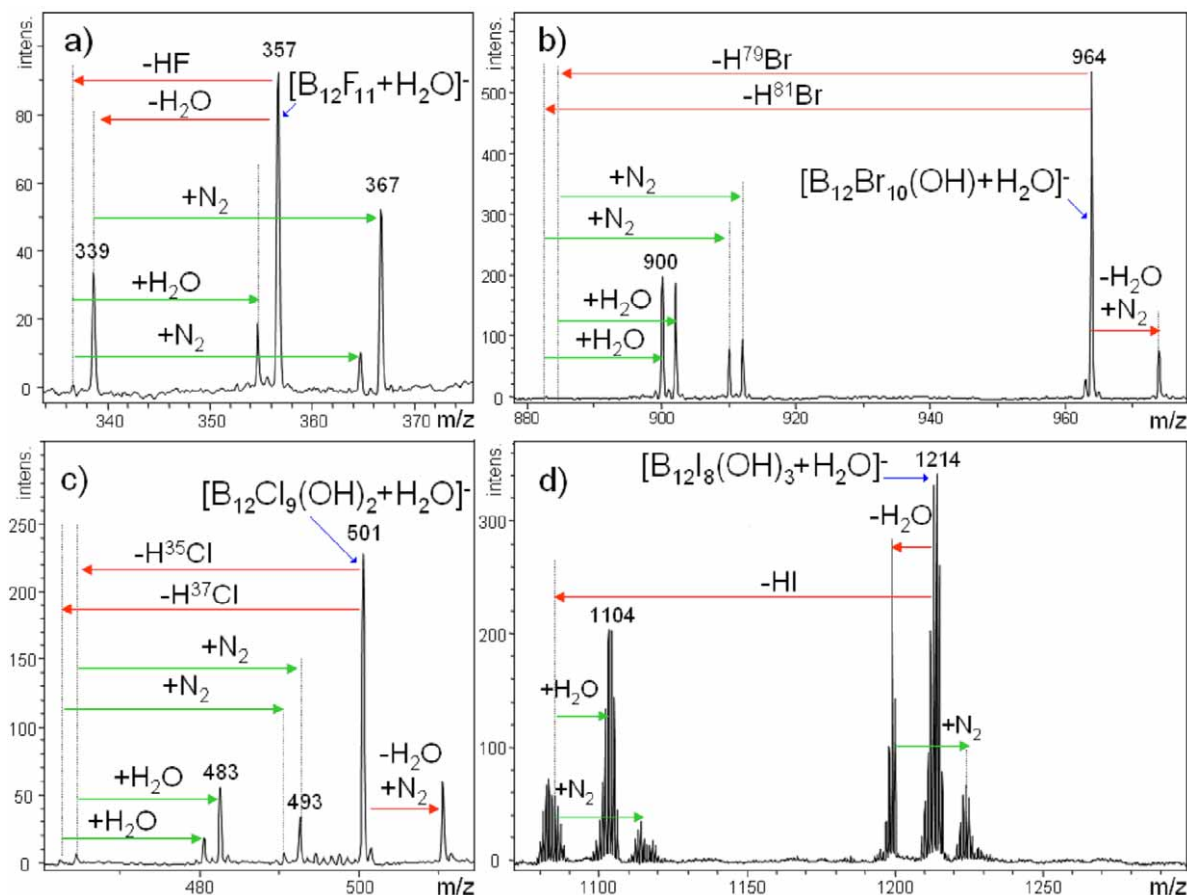
Fig. S7. ESI mass spectra showing the X-OH-substitution. Tandem-MS of a) all ions with nominal mass 357 of $[B_{12}F_{11} + H_2O]^-$; b) all ions with nominal mass 964 of $[B_{12}Br_{10}OH + H_2O]^-$; c) all ions with nominal mass 501 of $[B_{12}Cl_9(OH)_2 + H_2O]^-$ and d) all $[B_{12}I_8(OH)_3 + H_2O]^-$ ions.

S2. Spectra and detailed explanations to Scheme 2

$[B_{12}X_9]^-$ (X = Br, I) shows a complex sequence of reactions with the residual gases in the mass spectrometer. For X = I, the products of these reactions are only visible in the normal mass scan, because isolation of $[B_{12}I_9]^-$ leads to a dimerization reaction (cf. chapter 3.3). In contrast, for X = Br isolation of $[B_{12}Br_9]^-$ is possible (Fig. S8). Similar to the reactions of $[B_{12}X_{11}]^-$ successive substitution of X by OH is observed for $[B_{12}X_9]^-$ (X = Br, I). The formed ions all show the same reaction behavior (Fig. S6). The resulting spectra show a number of signals as a consequence of multiple reactions with the residual gases N_2 and H_2O in the mass spectrometer. The described reaction pathways were verified by tandem-MS measurements and reaction kinetic measurements (cf. chapter 1 and Fig. S4).
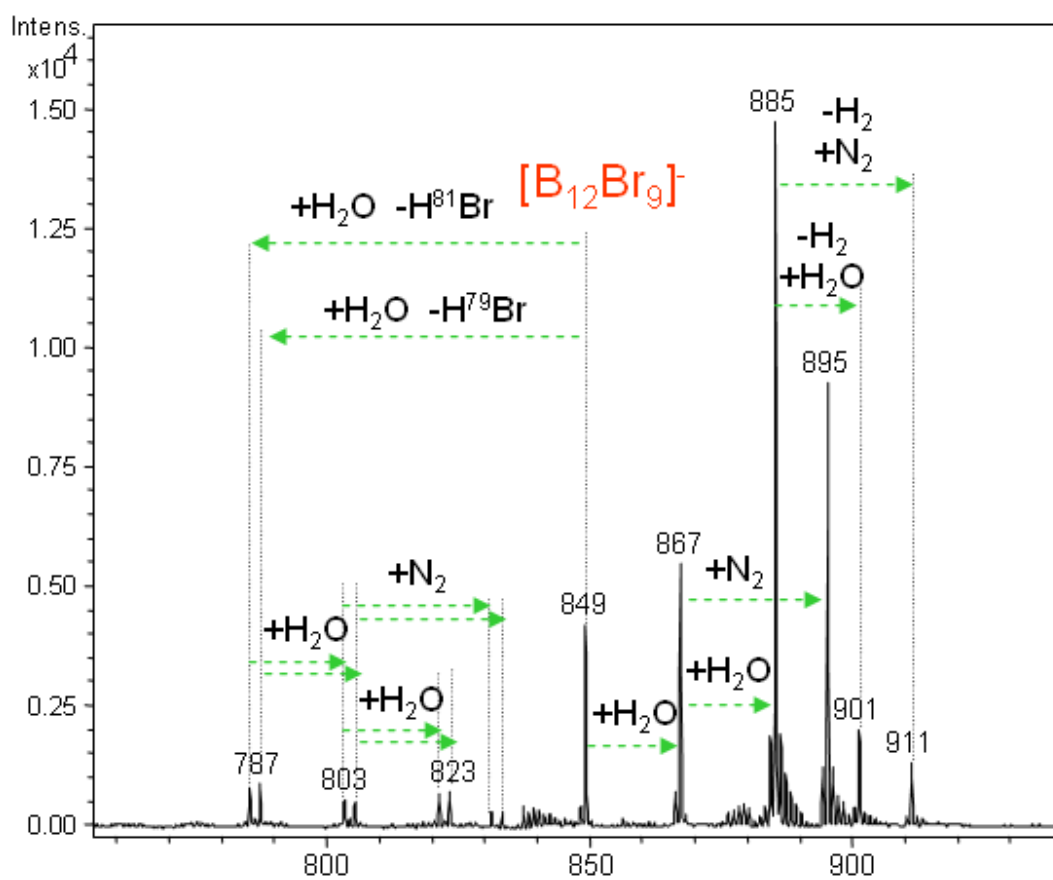
Fig. S8. ESI mass spectra showing the isolation of ions with nominal m/z-values 849 of $[B_{12}Br_9]^-$.
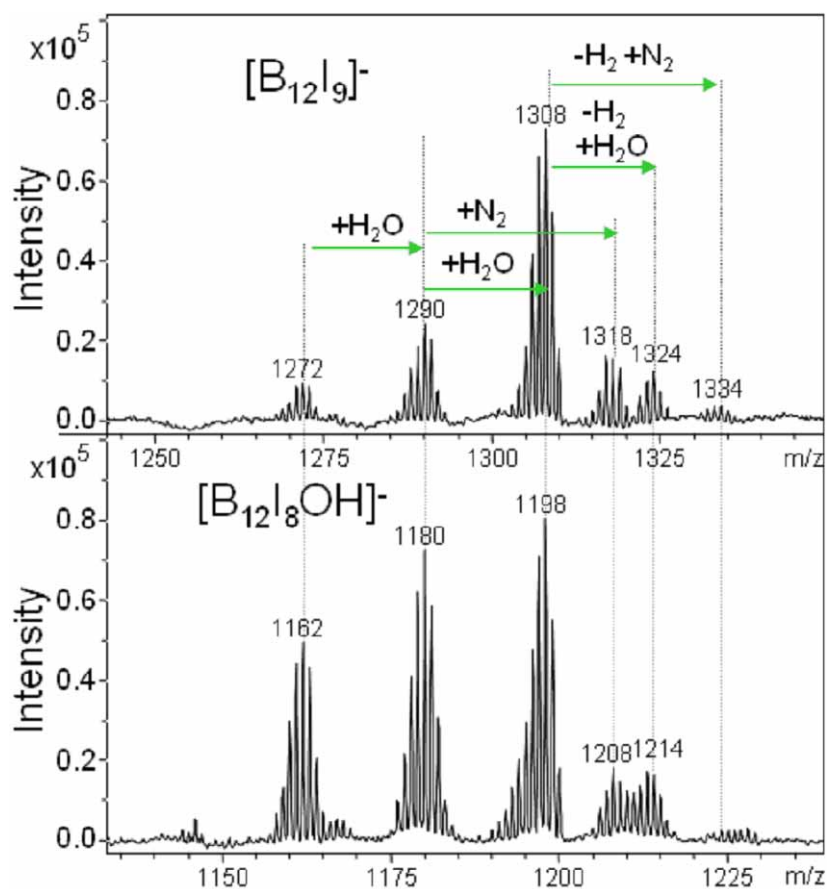
Fig. S9. ESI mass spectra comparing the reaction behavior of a) $[B_{12}I_9]^-$ and b) $[B_{12}I_8OH]^-$.

It can be expected that the mechanism of the X-OH substitution for $[B_{12}X_9]^-$ is similar to that suggested for $[B_{12}X_{11}]^-$ (Fig. 3). Thus, it is likely that the experimentally observed water adduct $[B_{12}X_{9-m}(OH)_m+H_2O]^-$ is an intermediate in this substitution sequence. Remarkably, tandem-MS experiments of this water adduct $[B_{12}X_{9-m}(OH)_m+H_2O]^-$ show signals for additional water and nitrogen adsorption products corresponding to those of an ion of type $[B_{12}X_{11-i}(OH)_i]^-$. Therefore, it is likely that the ions $[B_{12}X_{9-m}(OH)_m+H_2O]^-$, which are the reaction products of $[B_{12}X_{9-m}(OH)_m]^-$ and water are not simple adducts. It can be assumed that $[B_{12}X_{9-m}(OH)_m]^-$ still has an icosahedral structure, that the boron cluster is formally reduced due to previous loss of two halogen radicals and that there are three free coordination sites on the boron cluster. Thus, the reaction with H_2O could lead to a cleavage of the water molecule into an H- and an OH-ligand giving the ion $[B_{12}X_{9-m}(OH)_{m+1}H]^-$. This ion belongs to the type $[B_{12}X_{11-i}(OH)_i]^-$ with the only difference that there is one hydrogen ligand instead of a halogen ligand. Like a typical $[B_{12}X_{11-i}(OH)_i]^-$ ion, $[B_{12}X_{9-m}(OH)_{m+1}H]^-$ can adsorb water and nitrogen, which leads to the ions $[B_{12}X_{9-m}(OH)_{m+1}H + H_2O]^-$ and $[B_{12}X_{9-m}(OH)_{m+1}H + N_2]^-$. Consequently, the only difference

between the ions $[B_{12}X_{11-i}(OH)_i]^-$ and $[B_{12}X_{9-m}(OH)_{m+1}H]^-$, $[B_{12}X_{11-i}(OH)_i + H_2O]^-$ and $[B_{12}X_{9-m}(OH)_{m+1}H + H_2O]^-$, and $[B_{12}X_{11-i}(OH)_i + N_2]^-$ and $[B_{12}X_{9-m}(OH)_{m+1}H + N_2]^-$, respectively, is that the latter ones have a hydrogen ligand (compare Scheme 2). However, this difference leads to a different reaction behavior of the ions $[B_{12}X_{11-i}(OH)_i + H_2O]^-$ and $[B_{12}X_{9-m}(OH)_{m+1}H + H_2O]^-$. Whereas elimination of HX from $[B_{12}X_{11-i}(OH)_i + H_2O]^-$ requires some excitation energy, the ions $[B_{12}X_{9-m}(OH)_{m+1}H + H_2O]^-$ react nearly spontaneously by loss of the thermodynamically favored H_2 molecule and simultaneous formation of a $[B_{12}X_{11-i}(OH)_i]^-$ ion. Therefore, this branch of the pathway also winds up in the reaction pathway of the anionic ion pair shown in Scheme 1. Scheme S5 shows an detailed diagram for the periodinated cluster.
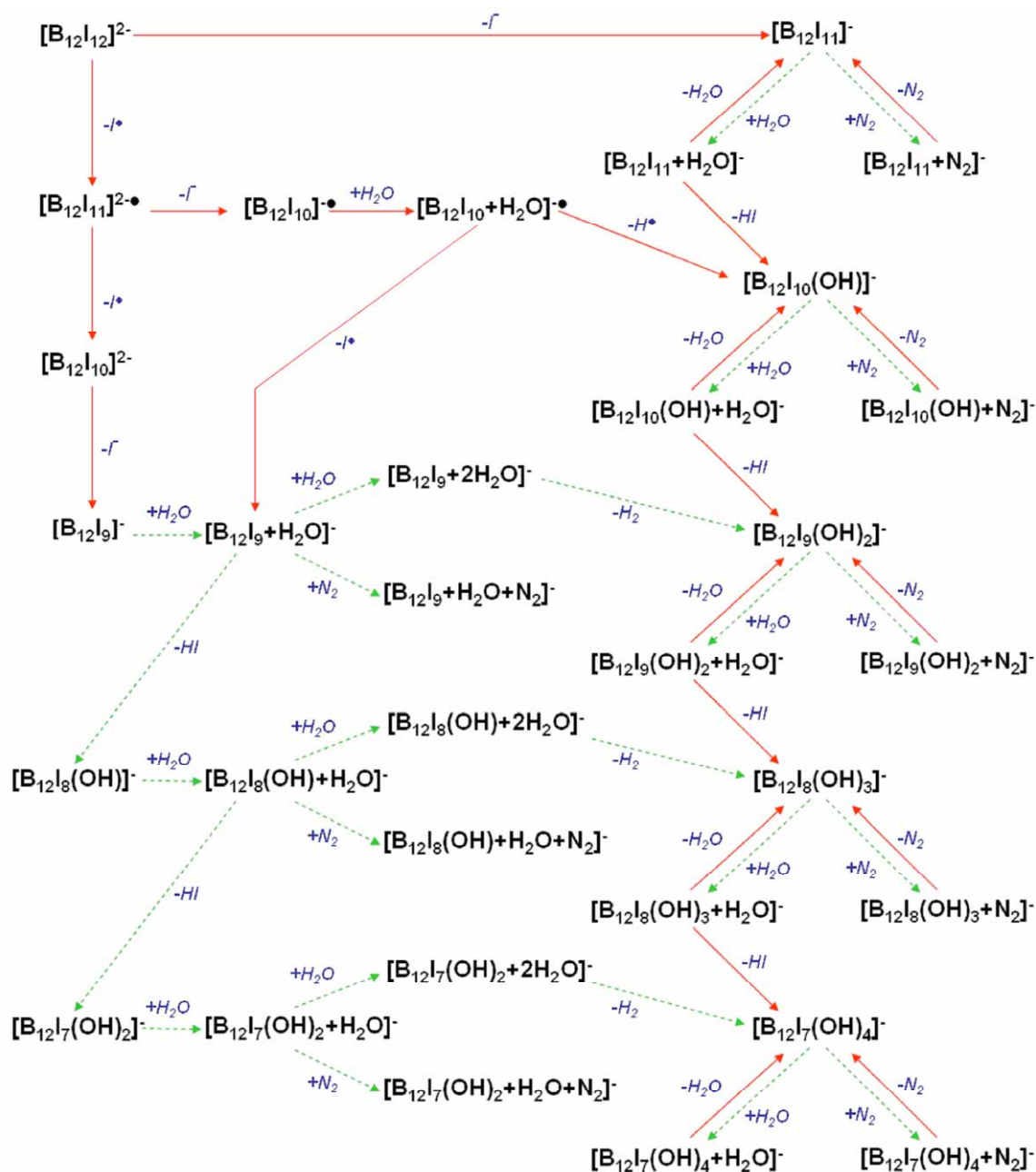
Scheme S5. Detailed reaction diagram for $[B_{12}I_{12}]^{2-}$ in an ion trap by applying excitation energy (for the legend compare Scheme 1).

S3. Additional information to chapter 3.3
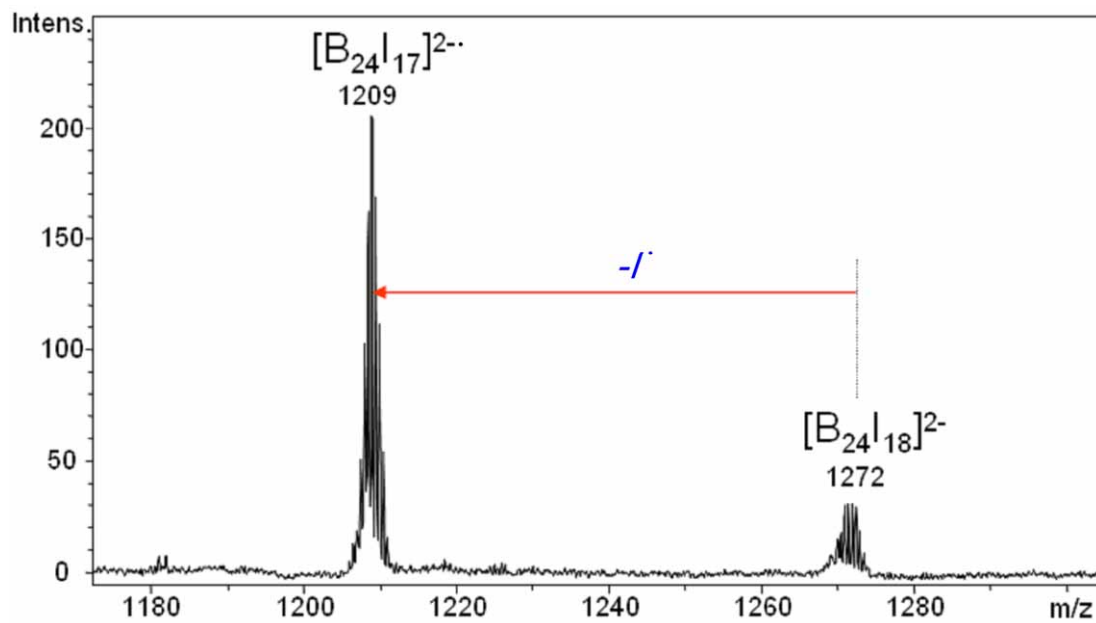
Fig. S10. ESI mass spectrum showing the elimination of an iodine radical from $[B_{24}I_{18}]^{2-}$ upon excitation.